in view of the different resonance enhancements of the various systems. Static β_{yyy} and β_{yxx} values are 452×10^{-30} and -300×10^{-30} e.s.u., respectively.

The experimental value of β for compound 3 is more than double that deduced by the additive model (that is, $\beta^{add}_{YYY} = 500 \times 10^{-30}$ e.s.u. compared to $1,200 \times 10^{-30}$ e.s.u. for the corresponding experimental value). This clearly indicates that the ruthenium atom in an octupolar geometry introduces an additional charge-transfer contribution to β on complexation of the three ligands by the metal, leading to an important enhancement of the nonlinearity as compared to that of the corresponding purely organic systems, as has been observed for more conventional dipolar species[18,19]. These results illustrate also the interest of three-dimensional organometallic structures as compared to rod-like geometries: enhancement of the octupolar part of the β tensor has led to β values in a magnitude range which has been previously believed to be unreachable for compounds other than one-dimensional dipolar systems. Moreover, large off-diagonal β_{YXX}, β_{XYX} and β_{XXY} tensor coefficients, which are equal to $-\beta_{YYY}$ in the case of octupolar molecules, are not available in the case of a one-dimensional tensor. Such multidirectional charge-transfer processes cooperate to enhance strongly the β tensor.

A current challenge is the macroscopic organization of nonlinear octupoles in non-centrosymmetric assemblies, remembering that electric field poling is precluded by the absence of permanent dipole moments. However, combined one-photon absorption at 2ω and two-photon absorption at ω (where ω is the fundamental frequency of a laser) will break the centrosymmetric order of the irradiated medium[20], resulting in a periodic absorption grating with quasi-phase-matching potential. The resulting 'octupolar' ordering can be 'frozen' by associating the combined absorption processes with reversible photoinduced effects[21,22]. □

Received 13 June 1994; accepted 15 February 1995.

1. Chemla, D. S. & Zyss, J. (eds) *Nonlinear Optical Properties of Organic Molecules and Crystals* (Academic, Boston, 1987).
2. Zyss, J. (ed.) *Molecular Nonlinear Optics: Materials, Physics and Devices* (Academic, Boston, 1993).
3. Zyss, J. *Nonlin. Opt.* **1,** 3–18 (1991).
4. Zyss, J. *J. chem. Phys.* **98,** 6583–6599 (1993).
5. Zyss, J. & Ledoux, I. *Chem. Rev.* **94,** 77–105 (1994).
6. Zyss, J., Dhenaut, C., Chau Van, T. & Ledoux, I. *Chem. Phys. Lett.* **206,** 409–414 (1993).
7. Verbiest, T. *et al. Opt. Lett.* **18,** 525 (1993).
8. Oudar, J-L. *J. chem. Phys.* **67,** 446–457 (1977).
9. Terhune, R. W., Maker, P. D. & Savage, C. M. *Phys. Rev. Lett.* **14,** 681–684 (1965).
10. Maker, P. D. *Phys. Rev.* A**1,** 923–951 (1970).
11. Cyvin, S. G., Rauch, J. E. & Decius, J. C. *J. chem. Phys.* **43,** 4083–4095 (1965).
12. Joffre, M., Yaron, D., Silbey, R. J. & Zyss, J. *J. chem. Phys* **97,** 5607–5615 (1992).
13. Barzoukas, M., Blanchard-Desce, M., Josse, D., Lehn, J-M. & Zyss, J. *Chem. Phys.* **133,** 323–329 (1989).
14. Blanchard-Desce, M., Lehn, J-M., Barzoukas, M., Ledoux, I. & Zyss, J. *Chem. Phys.* **181,** 281–289 (1994).
15. Rao, V. P., Jen, A. K. Y., Wong, K. Y. & Drost, K. J. *J. chem. Soc., chem. Commun.* 1118–1120 (1993).
16. Gilmour, S. *et al. Chem. Mater.* **6,** 1603–1604 (1994).
17. Juris, A. *et al. Coord. Chem. Rev.* **84,** 85–277 (1988).
18. Loucif-Saïbi, R. *et al. Chem. Phys.* **167,** 369–375 (1992).
19. Bourgault, M. *et al. J. chem. Soc. chem. Commun.* 1623–1624 (1993).
20. Nunzi, J-M., Charra, F., Fiorini, C. & Zyss, J. *Chem. Phys. Lett.* **219,** 349–354 (1994).
21. Charra, F., Kajzar, F., Nunzi, J-M., Raimond, P. & Idiart, E. *Opt. Lett.* **18,** 941–943 (1993).
22. Fiorini, C., Charra, F., Nunzi, J-M. & Zyss, J. in *Proc. Eur. Conf. Laser and Electro-optics* 33–34 (IEEE, Piscataway, 1994).
23. Juris, A., Campagna, S., Bidd, I., Lehn, J-M. & Ziessel, R. *Inorg. Chem.* **27,** 4007–4011 (1988).
24. Kocian, O., Mortimer, R. J. & Beer, P. D. *J. chem. Soc., Perkin Trans. I* 3203–3205 (1990).
25. Kelly, J. M., O'Connell, C. M. & Vos, J. G. *Inorg. Chim. Acta* **64,** L75–L76 (1982).
26. Sullivan, B. P., Salmon, D. J. & Meyer, T. J. *Inorg. Chem.* **17,** 3334–3341 (1978).

Prediction of crystal growth morphology based on structural analysis of the solid–fluid interface

X. Y. Liu*, E. S. Boek†, W. J. Briels‡ & P. Bennema*

* Department of Solid State Chemistry, University of Nijmegen, Toernooiveld 1, 6525 ED Nijmegen, The Netherlands
† Schlumberger Cambridge Research, High Cross, Madingley Road, Cambridge CB3 0EL, UK
‡ Chemical Physics Laboratory, University of Twente, PO Box 217, 7500 AE Enschede, The Netherlands

PREDICTING the shape of growing crystals is important for industrial crystallization processes. The equilibrium form of a crystal can be determined unambiguously from a consideration of the surface free energies of the various crystallographic faces $\{hkl\}$[1], but the growth morphology is determined by kinetic factors which are harder to predict. This morphology depends on the relative growth rates R^{rel}_{hkl} of the crystal faces. Several theories have been advanced[2,3] to relate R^{rel}_{hkl} to geometric or energetic characteristics of the surfaces $\{hkl\}$, but these have met with limited success in predicting the crystal morphologies observed. Here we present a theoretical approach to the problem in which R^{rel}_{hkl} is determined by quantities that are accessible either from kinetic models or from computer simulations of the solid–fluid interface. The important parameters controlling the growth rate are the energy required to create a step at the crystal surface and the free-energy barrier for an adsorbed solute molecule to be incorporated into the crystal. Both can be related to the mole fraction of adsorbed solute molecules in dynamic equilibrium with those in the crystal surface. When this approach is applied to the case of urea crystals grown from aqueous solution, we predict a needle-like shape which is consistent with experimental observations.

The growth of crystals bounded by facets usually occurs in a spiral fashion[4–7], whereby one or more screw dislocations on the crystal surface give rise to spiral steps (Fig. 1). Growth takes place by the deposition and incorporation of solute molecules from the bulk onto these steps, causing them to advance with a speed v_{step} along the surface, perpendicularly to the step (Fig. 1*a*, *b*). Denoting the average distance between two steps as λ_0 and their heights as d_{hkl}, the growth rate of the surface is given by $R_{hkl} = v_{step} d_{hkl}/\lambda_0$ (Fig. 1*b*). In the case of crystals grown from solutions, the delivery of molecules at the steps is governed by the diffusion of solute molecules from solution to the kinks[4] (Fig. 1*c*). In this process, the incorporation of these 'growth units' into kinks is rate-determining at relatively low supersaturations $\Delta\mu/kT$, and $v_{step} \propto X_{A(hkl)} \rho^{kink}_{hkl} \exp\{-\Delta G^{\ddagger}_{hkl}/kT\}$ for a given $\Delta\mu/kT$ (Fig. 1*c*). It follows that the relative growth rate of crystal faces $\{hkl\}$ is

$$R^{rel}_{hkl} \propto X_{A(hkl)} d_{hkl} \rho^{kink}_{hkl} \exp\{-\Delta G^{\ddagger}_{hkl}/kT\}/\lambda_0 \qquad (1)$$

where ρ^{kink}_{hkl} is the kink density, $X_{A(hkl)}$ is the solute concentration at the face (hkl), and $\Delta G^{\ddagger}_{hkl}$ is the activation free energy for adsorbed solute molecules to be incorporated into kinks. To relate the relative growth rate R^{rel}_{hkl} to quantities that can be easily obtained from a molecular-dynamics simulation, we introduce the concept of 'effective growth units'[8], which are those solute molecules adsorbed at the surface that are in dynamic equilibrium with the solid molecules at the kinks (called S^I molecules). All adsorbed solute molecules may be classified into two classes, F_1 and F_2. The former are those molecules that have roughly the same orientation or conformation as solid molecules at the surface (Fig. 3). To be incorporated into a kink, an F_1-molecule needs to surpass a barrier ΔG^{*}_{kink}, which corresponds to desolvation free energy. F_2 molecules are all other adsorbed solute molecules. Before they can be incorporated into

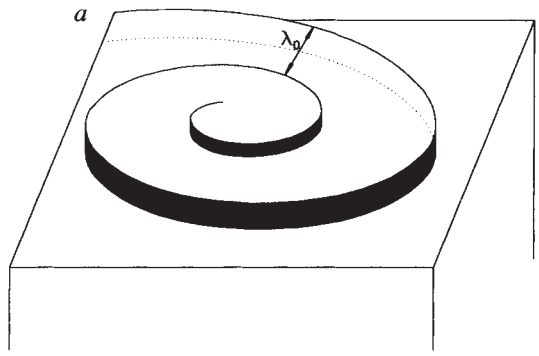

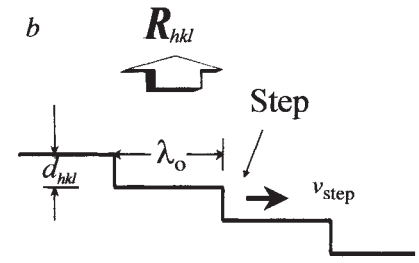

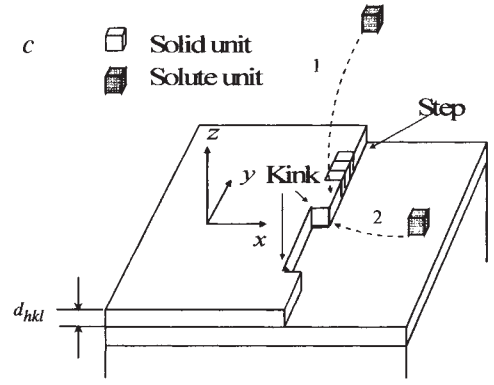

FIG. 1 *a*, Growth spiral for crystal surface growing from solution. The spiral is rotating with constant angular velocity under constant supersaturation $\Delta\mu/kT$ ($\Delta\mu=\mu^f-\mu^s$, where μ^f is the chemical potential of a solute molecule and μ^s of the solid molecule). The spiral is guided by the screw dislocation centre. Some distance from the centre, the spiral becomes roughly equal to concentric circular steps with a separation $\lambda_0\cong 19r_c$ (refs 4–7). Here r_c is the radius of the two-dimensional critical nucleus given by $r_c\approx\bar{\phi}_{step}\Omega/\Delta\mu$, $\bar{\phi}_{step}$ is the average step energy of a step per growth unit (compare with *c*) and Ω is the molecular volume. Therefore, $\lambda_0\propto\bar{\phi}_{step}$ at a given $\Delta\mu/kT$. *b*, From a two-dimensional cut through *a*, we see that the growth rate of a face (*hkl*), R_{hkl} is equal to the flux of steps given by $F_{step}=v_{step}\rho_{step}=v_{step}/\lambda_0$ times d_{hkl} (ρ_{step} is step density). So $R_{hkl}=d_{hkl}v_{step}/\lambda_o$. *c*, Surface model showing steps and kinks. A growth unit can be incorporated into the crystal structure at kink sites. The shape of v_{step} depends on the means of delivery of growth units to the steps[4]. For the growth of crystals from a solution, the surface diffusion of solute molecules to steps (route 2) is irrelevant, because the mean square displacement of an adsorbed solute molecule at the surface is short. Solute molecules are delivered directly from the bulk to steps at the surface by volume diffusion (route 1). This includes two main steps: the delivery of growth units to the steps by means of volume diffusion, and the integration of growth molecules into the crystal at kinks. At relatively low supersaturations, the latter is the rate determining step, and the rate is proportional to the concentration of adsorbed solute molecules $X_{A(hkl)}$ around the kinks, ρ_{hkl}^{kink} and $\exp\{-\Delta G_{hkl}^{\ddagger}/kT\}$. Therefore, $v_{step}\propto X_{A(hkl)}\rho_{hkl}^{kink}\exp\{-\Delta G_{hkl}^{\ddagger}/kT\}$ for a given $(\Delta\mu/kT)$ (ref. 4). The step energy ϕ_{step} (per structural unit) corresponds to the energy cost to create a step of a structural unit length. The kink energy ϕ_{kink} is then the energy cost to create a kink at a step. Assume that the step energy in the *x*-direction (shown here) is ϕ_x^{step}, and in the *y*-direction ϕ_y^{step}. It can easily be seen that ϕ_{kink} in the *x*-direction step is roughly equal to ϕ_y^{step}, and in the *y*-direction step is ϕ_x^{step}. If $\phi_x^{step}=\phi_y^{step}$, $\phi_{step}\approx\phi_{kink}$. Otherwise, the average step energy $\bar{\phi}_{step}$ is equal to the average kink energy $\bar{\phi}_{kink}$.

a kink, F_2 molecules must be transformed into F_1 molecules, for which they have to surpass a barrier ΔG^*. Effective growth units consist of F_1 molecules and those F_2 molecules for which ΔG^* is negligibly small. Two typical cases can be distinguished:

$\Delta G_{kink}^*>\Delta G^*$ (Fig. 2*a*). In this case both F_1 and F_2 molecules have equal probability of being incorporated into the kinks, and both are effective growth units. The mole fraction of effective growth units is $X_{A(hkl)}^{eff}\approx X_{A(hkl)}=X_{F_1}+X_{F_2}$.

$\Delta G_{kink}^*<\Delta G^*$ (Fig. 2*b*). In this case, F_2 molecules cannot be easily incorporated into the kinks and are not effective growth units. From the point of view of equilibrium thermodynamics, F_2 molecules may be said to be a separate species; in other words, the mole fraction of effective growth units is $X_{A(hkl)}^{eff}\approx X_{F_1}$.

Now we return to equation (1). To be incorporated into the kinks, adsorbed solute molecules should have the right orientation with respect to the solid molecules at the surface (refs 4, 5; X.Y.L. and P.B., manuscript in preparation). Given the definition of effective growth units, the probability for adsorbed solute molecules to obtain the proper orientation is about equal to $X_{A(hkl)}^{eff}/X_{A(hkl)}$, leading to the relation $\exp\{-\Delta G_{hkl}^{\ddagger}/kT\}\approx(X_{A(hkl)}^{eff}/X_{A(hkl)})\exp\{-\Delta G_{hkl}^{*}/kT\}$. ΔG_{hkl}^* is roughly independent of the specific surface[3,4], and can be considered a constant in this relationship.

The average separation of steps λ_0 is roughly proportional to the average step energy per molecule $\bar{\phi}_{hkl}^{step}$ (see Fig. 1*a* legend), and $\rho_{hkl}^{kink}\approx\exp\{-\bar{\phi}_{hkl}^{kink}/kT\}$ (refs 4–7). Because the average kink energy $\bar{\phi}_{hkl}^{kink}\approx\bar{\phi}_{hkl}^{step}$ (see Fig. 1*c* legend), $\rho_{hkl}^{kink}\approx\exp\{-\bar{\phi}_{hkl}^{step}/kT\}$. Combining the results so far, we find

$$R_{hkl}^{rel}\propto d_{hkl}X_{A(hkl)}^{eff}\exp\{-\bar{\phi}_{hkl}^{step}/kT\}/\bar{\phi}_{hkl}^{step} \qquad (2)$$

Obviously, to find the expression of $\bar{\phi}_{hkl}^{step}$ is one of the key issues. In the following, we shall arrive at

$$\bar{\phi}_{hkl}^{step}\approx\xi_{hkl}(\ln X_{A(hkl)}^{eff}/\ln X_A)\Delta H^{diss}/n_{hkl} \qquad (3)$$

Here n_{hkl} is the coordination number, that is, the number of neighbours of a solid molecule within the two-dimensional crystal slice (*hkl*), X_A is the concentration of solute molecules in the bulk, and ΔH^{diss} is the experimentally observed enthalpy of dissolution. The crystallographic orientation factor ξ_{hkl} will be defined below.

The step energy, the one-dimensional energy cost of creating a step with the length of one molecule, can be related to the three-dimensional local dissolution enthalpy ΔH_{hkl}^{diss} at the crystal surface (ref. 9; X.Y.L. and P.B., manuscript in preparation), which is the enthalpy change due to transforming a solid molecule at a kink to an adsorbed solute molecule. We may reduce ΔH_{hkl}^{diss} to a sum of in-plane contributions by multiplying it by $\xi_{hkl}=E_{hkl}^{slice}/E^{cr}$, where E^{cr} is the lattice energy per molecule and E_{hkl}^{slice} is the two-dimensional lattice energy per molecule for a crystal slice (*hkl*) with thickness d_{hkl} (ref. 3). We may approximate $\bar{\phi}_{hkl}^{step}n_{hkl}\approx\xi_{hkl}\times\Delta H_{hkl}^{diss}$. We notice that because of the ordering of fluid molecules at the interface and the crystal relaxation near the surface, ΔH_{hkl}^{diss} is normally different from ΔH^{diss} (ref. 9). Nevertheless, we may still easily estimate $\Delta H_{hkl}^{diss}/\Delta H^{diss}$ (ref. 9). From the van't Hoff relation[10] we have $\ln X_A=-\Delta H^{diss}/kT+\Delta H^m/kT^m\approx\Delta H^{diss}(T-T^m)/kTT^m$ (the superscript m denotes melting). Applying the same theories to the dissolution process at the crystal surface[9], we have $\ln X_{A(hkl)}^{eff}=-\Delta H_{hkl}^{diss}/kT+\Delta H_{hkl}^{m}/kT^m\approx\Delta H_{hkl}^{diss}(T-T^m)/kTT^m$. From the above relations we get $\Delta H_{hkl}^{diss}/\Delta H^{diss}\cong$

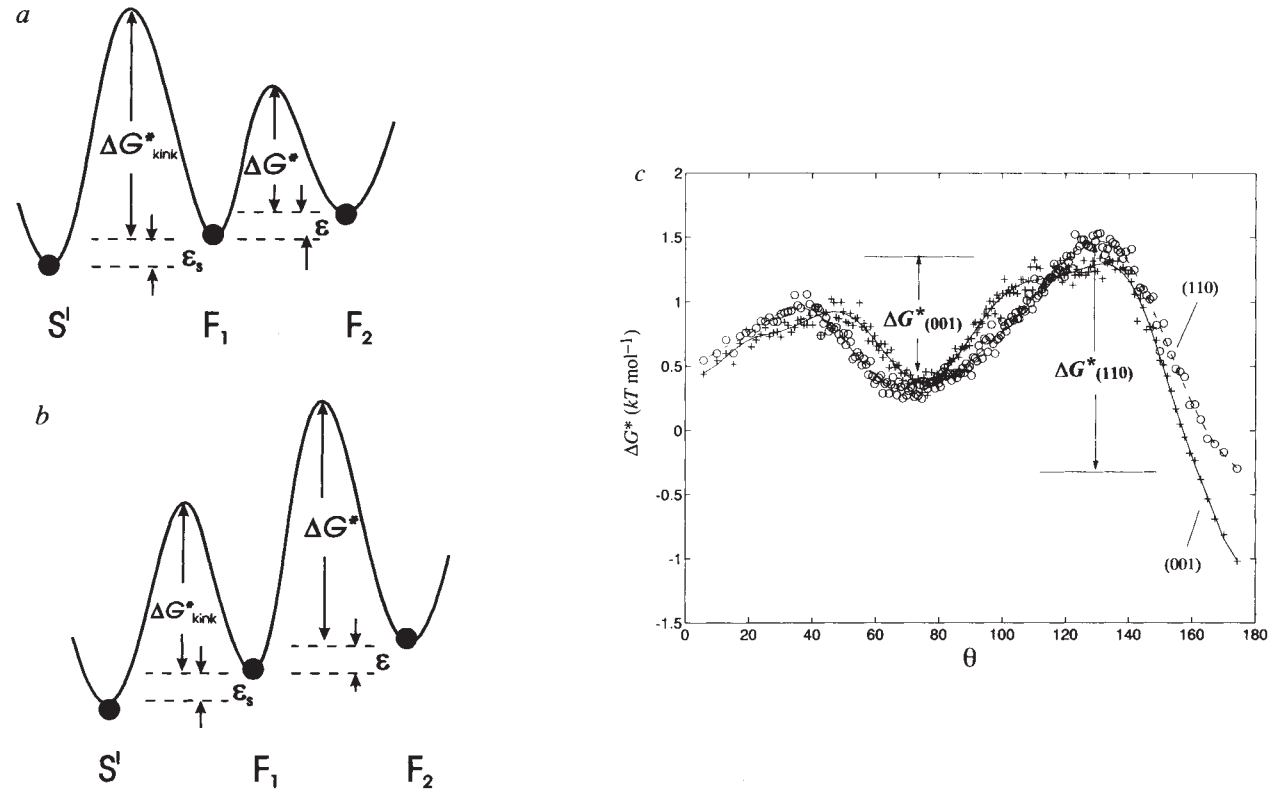

FIG. 2 *a* and *b*, The potential landscape between different types of structural units at the surface. In equilibrium with interfacial solid molecules S^I, F_1 molecules change directly into S^I molecules by passing the potential barrier ΔG^*_{kink}, while in a similar process, F_2 molecules should first change to F_1, and then to S^I molecules. (ΔG^* is the potential barrier for the transition from F_2 to F_1; $\varepsilon_s = \mu^0_{F_1} - \mu^0_{S^I}$, $\varepsilon = \mu^0_{F_2} - \mu^0_{F_1}$; μ^0 is the standard chemical potential for a certain species.) Thus, the rates of transition from a pure F_1 to an S^I molecule and from a pure F_2 to a pure F_1 molecule are given by $R^{I-S} = \nu_{F_1} \exp(-\Delta G^*_{kink}/kT)$ and $R^{II-I} = \nu_{F_2} \exp(-\Delta G^*/kT)$, respectively. Here ν_q denotes the frequency of thermal vibration of species q. So the rate of the transition from a pure F_2 to an S^I molecule is $R^{II-S} = R^{I-S}R^{II-I}/(R^{II-I} + R^{I-S})$. It is shown in *a* that $\Delta G^*_{kink} > \Delta G^*$, implying $R^{II-I} \gg R^{I-S}$ and $R^{II-S} \approx R^{I-S}$. In this case both F_1 and F_2 molecules can be treated as effective growth units. In *b*, it is shown that $\Delta G^*_{kink} < \Delta G^*$, implying that $R^{II-I} \ll R^{I-S}$ and $R^{II-S} \ll R^{I-S}$. In this case only F_1 molecules can be considered as the effective growth units. *c*, The potential of adsorbed urea molecules plotted against orientations of the dipole vectors of the molecules at the (001) interface (indicated by +) and the (110) interface (indicated by ○). The potential can be expressed as a function of the orientational distribution probability $P(\cos\theta)$ by $-kT \ln[P(\cos\theta)]$ (θ is the angle between the dipole vectors and the outward surface normal). The distribution probability $P(\cos\theta)$ has been calculated by averaging the time series of coordinates of the solute urea molecules in the first adsorbed liquid layer. For the orientation of (001) a small minimum at $\theta \approx 0$ in our present calculations correspond to the ordering of urea molecules occurring in the second fluid layer. The face (001) corresponds to case I (shown in *a*) and the face (110) corresponds to case Ii (shown in *b*). To determine the orientations of urea molecules fully, we should also look at the distribution of the N–N vector of urea molecules; similar analysis led to an extra factor of 0.5 in $X^{eff}_{A(hkl)}$ for {110} and 1 for {001}.

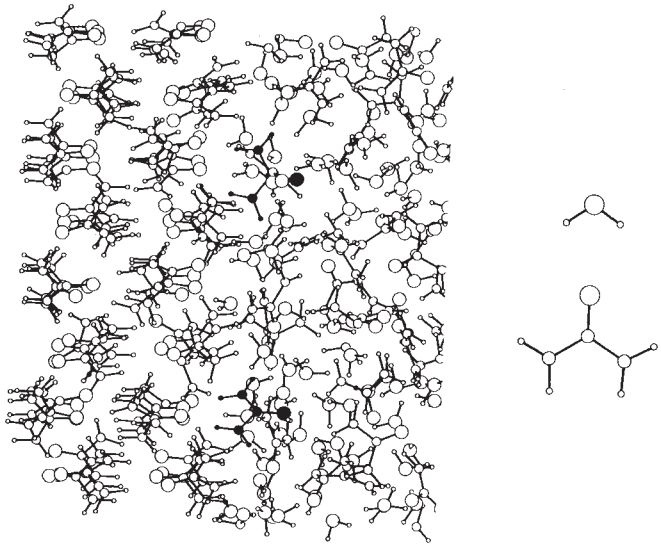

FIG. 3 Snapshot of the interface between crystalline urea (left) and saturated aqueous urea solutions (right) in the {001} orientations. On the right, a water molecule (above) and a urea molecule (below) are drawn for clarification. These snapshots have been generated by means of molecular dynamics simulations[15–17]. Using this technique, the newtonian equations of motion are integrated numerically for a large number of particles. The computational box consisted of 300 crystalline urea molecules, 200 solute urea molecules and 500 water molecules. Only the interfacial region of the computational box is shown. Simulation runs of about 200 picoseconds have been done for both interfaces. By averaging the time series of the generated coordinates, density profiles and orientational distributions of the adsorbed solute urea molecules at the interface have been calculated. Two F_1-like urea molecules in the first fluid layer of the (001) interface are drawn in black. (The intermolecular potentials chosen for the calculation are given in refs 15–17, and the self-consistency of the calculations has been checked by comparing the calculated total nitrogen radial distribution function with that of neutron scattering experiments[17]. The results are in good agreement.)

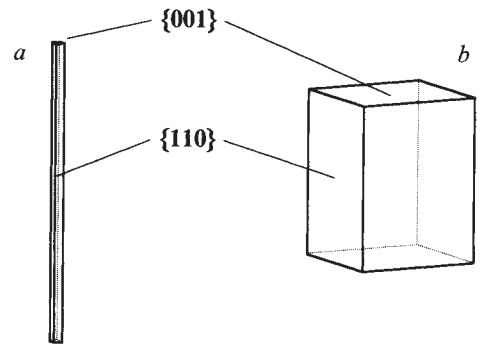

FIG. 4 Wulff constructions of the growth morphology of urea crystals based on different formalisms. *a*, The growth morphology predicted according to our approach (see equation (2)) ($R^{rel}_{001}/R^{rel}_{110} \approx 34.9$). *b*, The growth morphology predicted according to the Hartman–Perdok theory[3,11,18], where it was assumed that $R^{rel}_{hkl} \approx (1-\xi_{hkl})$ ($R^{rel}_{001}/R^{rel}_{110} \approx 1.35$). The growth habits of urea crystals shown in *a* and *b* are substantially different. One is needle-like, the other is block-like. Experiments[13,14] show that urea crystals grown from aqueous solutions have a needle-like shape ($R^{rel}_{001}/R^{rel}_{110} \approx 50$). $d_{001} = 4.712$ Å, $d_{110} = 4.003$ Å (ref. 12); $\xi_{001} = 0.556$, $\xi_{110} = 0.671$ (ref. 18); $n_{001} \approx n_{110} \approx 4$ (ref. 18); $X^{eff}_{A(001)} \approx 0.031$, $X^{eff}_{A(110)} \approx 0.088$ (this work); $X_A = 0.256$ (ref. 17), and $\Delta H^{diss}/kT = 6.79$ ($T = 298.15$ K) (ref. 19).

$\ln X^{eff}_{A(hkl)}/\ln X_A$ (ref. 9), from which we finally obtain equation (3). Thus, the growth rate of a specific crystal face can be determined from equations (2) and (3). The quantities n_{hkl}, d_{hkl} and ξ_{hkl} can easily be calculated from the crystal structure and a given potential model (refs 3, 11 and X.Y.L. and P.B., manuscript in preparation). The key issue then is to calculate $X^{eff}_{A(hkl)}$ from an analysis of the interfacial structure obtained from molecular dynamics simulations.

We now apply the above theory to urea crystals grown from aqueous solutions. Urea ($O{=}C(NH_2)_2$) crystallizes in the tetragonal space group $P_{\bar{4}2_1m}$ ($a = 5.661$, $c = 4.712$ Å)[12]. According to experiments[13,14] the crystals are mainly bounded by the {001}, the {110} and the {111} faces. We shall ignore the {111} faces for the sake of simplification. To calculate $X^{eff}_{A(hkl)}$ and $X_{A(hkl)}$ for the remaining two surfaces, we have carried out molecular dynamics simulations[15–17] for the two interfaces between a saturated urea solution and the crystal surfaces, at $X_A = 0.256$. A snapshot along the interface of {001} is shown in Fig. 3. Potential distributions of the dipole vectors (O→C) of solute urea at the surfaces of {001} and {110} are shown in Fig. 2*c*.

F_1 urea molecules in the first fluid layer at the {001} surfaces should have their O→C dipoles roughly antiparallel to the outward surface normal ($\theta \approx 180°$), where θ is the angle between the vectors and the outward surface normal; see Fig. 3). In Fig. 2*c*, an eminent minimum occurs at $\theta \approx 180°$. The transformation from other orientations to the orientation of $\theta \approx 180°$ may need to pass at most the small potential barrier $\Delta G^*_{(001)}$ ($\leqslant 1\,kT$). It can be roughly estimated[4] that $\Delta G^*_{kink} \approx kT$. This suggests that ΔG^* is small compared with ΔG^*_{kink}, and we have the case where $X^{eff}_{A(001)} \approx X_{A(001)}$.

Unlike the {001} faces, F_1-like urea molecules at the {110} faces should have their O→C dipoles roughly parallel to the surface ($\theta \approx 90°$)[15,18]. It is shown in Fig. 2*c* that $\Delta G^*_{(100)}$ is relatively high ($\Delta G^*_{(110)} \approx 2\Delta G^*_{(001)}$), so here we have the second case. Only those urea molecules with $60° \leqslant \theta \leqslant 120°$ are regarded as F_1-like molecules or effective growth units. (ΔG^* of those molecules are equal to or less than zero; see Fig. 2*c*). From $X_{A(110)}$ and Fig. 2*c*, $X^{eff}_{A(110)}$ can be calculated.

Substituting these data, together with n_{hkl}, d_{hkl} and ξ_{hkl} (refs 12, 18), into equations (2) and (3) yields R^{rel}_{hkl} for the two orientations (see Fig. 4 legend for details). The growth form of urea crystals is constructed based on R^{rel}_{hkl} in corresponding crystallographic orientations[1,3]. We predict that, in the case of growth from aqueous solution, urea crystals should adopt a needle-like shape (Fig. 4*a*), in agreement with experimental observations[12,13]. This striking result demonstrates the validity of our approach in the prediction and the study of morphology of crystals growing from solutions. □

Received 23 September 1994; accepted 7 February 1995.

1. Kern, R. in *Morphology of Crystals* (ed. Sunagawa, I.) 77–206 (Terra, Tokyo, 1987).
2. Donnay, J. D. H. & Harker, D. *Am. Mineral.* **22,** 446–447 (1937).
3. Hartman, P. in *Morphology of Crystals* (ed. Sunagawa, I.) 269–319 (Terra, Tokyo, 1987).
4. Chernov, A. A. *Modern Crystallography III—Crystal Growth* 1–158 (Springer, Berlin, 1984).
5. Bennema, P. & Gilmer, J. in *Crystals Growth: An Introduction* (ed. Hartman, P.) 263–327 (North Holland, Amsterdam, 1973).
6. Burton, W. K., Cabrera, N. & Frank, F. C. *Phil. Trans. R. Soc.* **243,** 299–358 (1951).
7. Ohara, M. & Reid, R. C. *Modeling Crystal Growth Rates from Solution* 1–165 (Prentice-Hall, Englewood Cliffs, 1973)
8. Liu, X. Y. & Bennema, P. *Phys. Rev.* B**49,** 765 (1994).
9. Liu, X. Y. & Bennema, P. *J. chem. Phys.* **98,** 5863–5875 (1993); Liu, X. Y. & Bennema, P. in *Current Topics in Crystal Growth Research* (in the press).
10. Fowler, S. R. & Guggenhein, E. A. *Statistical Thermodynamics* (Cambridge, London, 1960).
11. Bennema, P. in *Handbook on Cryst. Growth* (ed. Hurle, D. T. J.) 477–581 (North-Holland, Amsterdam, 1993).
12. Worsham, J. E., Levy, J. H. A. & Peterson, S. W. *Acta cryst.* **10,** 319 (1957).
13. Davey, R., Fila, W. & Garside, J. *J. Crystal Growth* **79,** 607–613 (1986).
14. Docherty, R., Roberts, K. J., Saunder, V., Black, S. & Davey, R. J. *Faraday Discuss.* **95,** 11–25 (1993).
15. Boek, E. S., Briels, W. J., van Eerden, J. & Feil, D. *J. chem. Phys.* **96,** 7010–7018 (1992).
16. Boek, E. S., Briels, W. J. & Feil, D. *J. phys. Chem.* **98,** 1674–1681 (1994).
17. Boek, E. S., Briels, W. J. & Feil, D. *J. chem. Phys.* **98,** 1422–1428 (1993).
18. Boek, E. S., Feil, D., Briels, W. J. & Bennema, P. *J. Crystal Growth* **114,** 389–410 (1991).
19. Pickering, M. *J. Chem. Education* **64,** 723–724 (1987).

Chiral discrimination of monosaccharides using a fluorescent molecular sensor

Tony D. James, K. R. A. Samankumara Sandanayake & Seiji Shinkai*

Chemirecognics Project, ERATO, Research Development Corporation of Japan, Aikawa 2432-3, Kurume, Fukuoka 830, Japan

MEANS of distinguishing between enantiomers of a chiral molecule are of critical importance in many areas of analytical chemistry and biotechnology, particularly in drug design and synthesis. In particular, solution-based sensor systems capable of chiral recognition would be of tremendous pharmaceutical value. Here we report the chiral discrimination of D- and L-monosaccharides using a designed receptor molecule that acts as a sensor by virtue of its fluorescent response to binding of the guest species. Our receptor contains boronic acid groups that bind saccharides by covalent interactions; such receptor systems have been much studied previously[1–6] for complexation of saccharides, and have an advantage over others based on hydrogen-bonding interactions[7–11], for which polar protic solvents such as water can compete with guest binding. Our molecular sensor also incorporates a fluorescent naphthyl moiety; binding of each enantiomer of the monosaccharides alters the fluorescence intensity to differing degrees, enabling them to be distinguished. These water-soluble molecular sensors might form the basis of a quantitative and selective analytical method for saccharides.

Recently we developed a photoinduced-electron-transfer (PET)[12,13] sensor for saccharides based on the interaction of boronic acid and amines[2,3]. When saccharides form cyclic boronate esters with boronic acids such as **1** and **2** (Fig. 1), the acidity of the boronic acid is enhanced[14] and therefore the Lewis acid–base interaction with the tertiary amine is strengthened. The strength of this acid–base interaction modulates the photoinduc-

* To whom correspondence should be addressed.